Dynamos in partially convective M dwarfs

B. Toro-Velásquez[1], D.R.G. Schleicher[1], P.J. Käpylä[2], C.A. Ortiz-Rodríguez[3], F.H. Navarrete[4], & J.P. Hidalgo[1]

[1] *Departamento de Astronomía, Universidad de Concepción, Chile*
[2] *Institut für Sonnenphysik, KIS, Alemania*
[3] *Hamburger Sternwarte, Universität Hamburg, Alemania*
[4] *Institute of Space Sciences, ICE–CSIC, España*

Received: 09 February 2024 / Accepted: 19 March 2024

Resumen / Las enanas M son estrellas de baja masa de la secuencia principal, el tipo de estrella más común de la galaxia. Es bien sabido que tienen una importante actividad magnética, pero el mecanismo que la controla aún no está claro. Las enanas M con masas mayores a 0.35 $M_\odot$ son parcialmente convectivas, y esta transición marca un importante cambio en la estructura estelar que puede afectar a la producción y almacenamiento de campos magnéticos internos. El objetivo de este trabajo es probar un nuevo modelo computacional para la dínamo de enanas M parcialmente convectivas. Este modelo consiste en simulaciones numéricas magnetohidrodinámicas tridimensionales utilizando el modelo de estrella en una caja, donde consideramos una estrella de radio R en un cubo cartesiano de tamaño $(2.2R)^3$. Dentro de este modelo, cambiamos las condiciones magnéticas de contorno para estudiar cómo esto puede afectar a la dínamo; además se exploraron diferentes velocidades de rotación.

Abstract / M dwarfs are low-mass main-sequence stars, which are the most common type of star in the galaxy. It is well know that they have significant magnetic activity but the mechanism that controls is still unclear. M dwarfs more massive than 0.35 $M_\odot$ are partially convective and this transition marks an important change in the stellar structure that can affect the production and storage of internal magnetic fields. The aim of this work is to test a new computational model for the dynamos of partially convective M dwarfs. This model consists of three-dimensional magnetohydrodynamical numerical simulations using a star-in-a-box model, where we consider a star of radius R in a Cartesian cube of size $(2.2R)^3$. Within this model, we change the magnetic boundary conditions to see how this affects the dynamo and also explore different rotation rates.

Keywords / stars: magnetic field — dynamo — magnetohydrodynamics (MHD) — stars: low-mass

1. Introduction

Dynamo theory describes the process through which a rotating, convecting, and electrically conducting fluid generate and maintain a magnetic field. This theory is used to explain the presence of long-lived magnetic fields in astrophysical bodies (Brandenburg, 2007). In stars, the conductive fluid is the ionized gas in the convective zone and at the tachocline, which is the transition region between the radiative and convective zones.

M dwarfs are low-mass late-type main sequence stars, which are the most common type of stars in the galaxy (Winters et al., 2019), and which often show significant magnetic activity (Kochukhov, 2021). The stellar mass determines the structure of M dwarfs which range from 0.08 to 0.55 $M_\odot$. If the M dwarf has a mass greater than 0.35 $M_\odot$, the star is partially convective, which means that it has a radiative core and a convective envelope. If the stellar mass is less than 0.35 $M_\odot$, the star is fully convective (Chabrier & Baraffe, 1997).

Several models have been developed to study stellar dynamos, some of which consider fully convective stars. Most of these simulations operate in spherical shells, (e.g., Brown et al. 2020; Warnecke et al. 2016). Another option is to use the star-in-a-box model (e.g., Ortiz-Rodríguez et al. 2023; Käpylä 2021). Whereas other works model partially convective stars, such as sun-like stars (e.g., Navarrete et al. 2018, 2020). Käpylä (2022) applied a star-in-a-box model to solar-like stars in a recent study. Our goal is to apply the star-in-a-box setup for partially convective M dwarfs to study the behavior of the magnetic fields within the star. In Käpylä (2022), different rotation rates were used and it was noted that while the exact excitation mechanism of the dynamos in the current simulations is not yet clear, it was shown that the including a radiative core and regions exterior to the star are important in shaping the dynamo.

As a consequence, in this work we present 3D magnetohydrodynamical (MHD) numerical simulations of partially convective M dwarf stars at different rotations rates, where we changed the magnetic boundary conditions in the exterior of the star to study how this affects the dynamo. First, we present the computational methods used with a brief description of the model and the stellar parameters in section 2 and then we show the preliminary results in section 3. We finish with the conclusions and future work in section 4.

✉ *Contact* / btoro2017@udec.cl

Research article

2. Computational methods

2.1. The Pencil Code

The simulations were run with the PENCIL CODE* (Pencil Code Collaboration et al., 2021) which is a high-order finite-difference code for compressible hydrodynamics with magnetic fields. The code can solve both ordinary and partial differential equations, and it is easily adapted to different types of problems by activating or deactivating the different modules as needed. The code uses parallel domain decomposition and MPI.

2.2. The Model

The star-in-a-box model is described in Käpylä (2021), and is based on the set-up of Dobler et al. (2006). We consider a sphere of radius R that is enclosed in a Cartesian cube with side $H = 2.2\ R$ where all coordinates (x, y, z) range from $-H/2$ to $H/2$. The equations to solve are the induction, continuity, momentum, and energy conservation equations, given respectively by

$$\frac{\partial \mathbf{A}}{\partial t} = \mathbf{U}\times\mathbf{B} - \eta\mu_0\mathbf{J}, \tag{1}$$

$$\frac{\mathrm{D}\ln\rho}{\mathrm{D}t} = -\boldsymbol{\nabla}\cdot\mathbf{U}, \tag{2}$$

$$\frac{\mathrm{D}\mathbf{u}}{\mathrm{D}t} = -\nabla\Phi - \frac{1}{\rho}(\nabla p - \nabla\cdot 2\nu\rho\boldsymbol{S} + \mathbf{J}\times\mathbf{B}) - 2\boldsymbol{\Omega}\times\mathbf{U} + f_d, \tag{3}$$

$$T\frac{\mathrm{D}s}{\mathrm{D}t} = -\frac{1}{\rho}[\nabla\cdot(\mathbf{F}_{\rm rad}+\mathbf{F}_{\rm SGS}) + \mathcal{H} - \mathcal{C}] + 2\nu\mathbf{S}^2 + \mu_0\eta\mathbf{J}^2, \tag{4}$$

where $\mathbf{A}$ is the magnetic vector potential, $\mathbf{U}$ is the velocity, $\mathbf{B} = \nabla\times\mathbf{A}$ is the magnetic field, $\mathbf{J} = \boldsymbol{\nabla}\times\mathbf{B}/\mu_0$ is the current density, μ_0 is the permeability of vacuum, η is the magnetic diffusivity, $\mathrm{D}/\mathrm{D}t = \partial/\partial t + \mathbf{U}\cdot\boldsymbol{\nabla}$ is the advective derivative, ρ is the fluid density, Φ is the gravitational potential, p is the pressure, ν is the kinematic viscosity, $\mathbf{S}$ is the traceless rate-of-strain tensor. $\mathcal{H}$ and $\mathcal{C}$ describe heating and cooling, and f_d describes the damping of flows outside the star. $\boldsymbol{\Omega} = (0, 0, \Omega_0)$ is the rotation rate of the star, T is the temperature, s is the specific entropy, $\mathbf{F}_{\rm rad}$ is the radiative flux and $\mathbf{F}_{\rm SGS}$ is the subgrid-scale (SGS) entropy flux. These last two expressions are respectively

$$\mathbf{F}_{\rm rad} = -K\nabla T, \tag{5}$$

$$\mathbf{F}_{\rm SGS} = -\chi_{\rm SGS}\rho\nabla s', \tag{6}$$

where K corresponds to Kramers opacity law, $\chi_{\rm SGS}$ is the SGS diffusion coefficient, $s' = s - \bar{s}_t$ is the entropy fluctuation and $\bar{s}_t$ is a running temporal mean of the entropy.

2.3. Stellar parameters

Due to the fully compressible formulation of the MHD equations, we use a much higher luminosity than in the target star to avoid the time step being limited by sound waves and to resolve the Kelvin-Helmholtz timescale. Therefore, the results must be scaled to represent them in physical units; see Käpylä et al. (2020).

For the conversion to physical units we need the parameters of a reference star. In this case we use a star simulated with the stellar evolution code MESA (Paxton et al., 2019) with its online version MESA web**. In particular, we simulate a star of $M_\star = 0.75\ M_\odot$, $R_\star = 0.72\ R_\odot$, $L = 0.94\ L_\odot$ and $\rho_c^\star = 1.08\times10^5$ kg m^{-3}. Following the description in Appendix A of Käpylä et al. (2020) we calculate the dimensionless luminosity. In the current simulation we have $\mathcal{L} = 5.8\times10^{-5}$ and the value from the target star is $\mathcal{L}_\star = 1.36\times10^{-12}$. Thus, the velocities are enhanced by a factor $L_{\rm ratio}^{1/3} \approx 350$, where $L_{\rm ratio} = \mathcal{L}/\mathcal{L}_\star \approx 4.3\times10^7$.

The surface gravity of the star is

$$g_\star = \frac{GM_\star}{R_\star^2} = \frac{0.75}{(0.72)^2}\frac{GM_\odot}{R_\odot^2} \approx 1.45\ g_\odot \approx 396\ \mathrm{m\,s^{-2}},$$

where $g_\odot = 274\ \mathrm{m\,s^{-2}}$. For the rotation rate conversion factor we have

$$\Omega^{\rm sim} = L_{\rm ratio}^{1/3}\left(\frac{g^{\rm sim}}{g_\star}\frac{R_\star}{R^{\rm sim}}\right)^{1/2}\Omega_\star,$$

using the solar rotation rate $\Omega_\star = \Omega_\odot = 2.7\times10^{-6}$ s^{-1}, yields

$$\Omega^{\rm sim} = 1.062\left(\frac{g^{\rm sim}}{R^{\rm sim}}\right)^{1/2},$$

where $g^{\rm sim} = g^{\rm sim}(r = R) \approx 1$ and $R^{\rm sim} = 1$ in simulation units. After substitution and conversion to physical units (Mm, yr, and kG), we get conversions factors

$$x\ [\mathrm{Mm}] \approx 500\ x^{\rm sim}\ [\mathrm{sim.units}], \tag{7}$$

$$t\ [\mathrm{yr}] \approx 0.0125\ t^{\rm sim}\ [\mathrm{sim.units}], \tag{8}$$

$$U\ [\mathrm{m\,s^{-1}}] \approx 1271.2\ U^{\rm sim}\ [\mathrm{sim.units}], \tag{9}$$

$$B\ [\mathrm{kG}] \approx 4691\ B^{\rm sim}\ [\mathrm{sim.units}]. \tag{10}$$

2.4. Simulation Parameters

The opacity of the medium is described by Kramers opacity law (Brandenburg et al., 2000). We choose the value of the opacity so that we have a radiative core and a convective envelope. We use different Ω for sets B, C, D and E, and three different setups are explored: in the first one (B1, C1, C5) $\nu = \eta$, in the second one (B2, C2, C3, D1, E1) diffusivity profiles are added inside of the star, and in the third one (B3, C4) the diffusivity profiles are added both inside and outside the star; see Table 1 for values. We use smaller values of η and ν at the center of the star, which are 5×10^{-7} and 2.5×10^{-7} respectively. In the second case, we decreased the value of η and ν (mentioned above) by a factor 10^2 below the tachocline, which is situated at about $r = 0.6R$ (first jump). For the third case, we consider the jump inside the star mentioned before, and add a second jump in the

*https://pencil-code.org/

**http://user.astro.wisc.edu/~townsend/static.php?ref=mesa-web-submit

Table 1. Summary of the simulation. From left to right the columns correspond to the simulation name, angular velocity, $\nu_{\rm cz}$, $\eta_{\rm cz}$ and $\eta_{\rm ext}$ are the kinematic viscosity and the magnetic diffusivity in the convective zone of the star, and the value of magnetic diffusivity outside the star, respectively. Then, we have the dimensionless numbers, which are the magnetic Prandtl number, its value in the exterior of the star, and the SGS Prandtl number, the magnetic Reynolds number inside the star, and its value in the exterior of the star, and the fluid Reynolds number, respectively. The last two columns indicate the Coriolis number and grid resolution, respectively. * indicate runs with diffusivity profile inside of the star and ** indicate runs with a different value of η in the exterior of the star.

Run	Ω	$\nu_{\rm cz}$	$\eta_{\rm cz}$	$\eta_{\rm ext}$	${\rm Pr_M}$	${\rm Pr_{Me}}$	${\rm Pr_{SGS}}$	${\rm Re_M}$	${\rm Re_{Me}}$	Re	Co	Grid
B1	1.0	1.0×10^{-4}	1.0×10^{-4}	–	1.0	–	0.2	13.66	–	13.66	5.93	128^3
B2*	1.0	2.5×10^{-5}	5.0×10^{-5}	–	0.5	–	0.05	31.34	–	62.69	5.17	128^3
B3**	1.0	2.5×10^{-5}	5.0×10^{-5}	5.0×10^{-4}	0.5	0.05	0.05	30.69	3.07	61.39	5.28	200^3
C1	2.0	1.0×10^{-4}	1.0×10^{-4}	–	1.0	–	0.2	11.64	–	11.64	13.93	128^3
C2*	2.0	2.5×10^{-5}	5.0×10^{-5}	–	0.5	–	0.05	33.79	–	67.57	9.60	128^3
C3*	2.0	2.5×10^{-5}	5.0×10^{-5}	–	0.5	–	0.05	26.16	–	52.31	12.40	200^3
C4**	2.0	2.5×10^{-5}	5.0×10^{-5}	5.0×10^{-4}	0.5	0.05	0.05	25.52	2.55	51.03	12.71	200^3
C5	2.0	1.5×10^{-4}	1.5×10^{-4}	–	1.0	–	0.6	7.09	–	7.09	15.25	128^3
D1*	3.0	2.5×10^{-5}	5.0×10^{-5}	–	0.5	–	0.05	22.95	–	45.90	21.19	288^3
E1*	5.0	2.5×10^{-5}	5.0×10^{-5}	–	0.5	–	0.05	16.89	–	33.77	48.00	288^3

η parameter, by a factor 10^3 respect to the core value, outside of the star, i.e., $R > 1.0$. The standard case with ${\rm Pr_M} = 1$ is chosen because it is numerically the most convenient. The justification to lower the diffusivity in the core is to slow down the diffusion of flows and magnetic fields from the convection zone to the core. Similarly the profile exterior to the star prevents too rapid diffusion and effectively changes the boundary condition of the magnetic field at the surface of the star.

2.5. Dimensionless numbers

Table 1 shows the values of different dimensionless numbers which help us to characterize each of the simulations. Here the quantities are evaluated in the convective zone of the star, so the scale of the largest convective eddies is given by $k_R = 2\pi/0.4R$.

The Coriolis number is a measure of the influence rotation on the flow

$$\mathrm{Co} = \frac{2\Omega_0}{u_{\rm rms} k_R}, \tag{11}$$

where $u_{\rm rms}$ is the volume-averaged root-mean-square velocity. The fluid and magnetic Reynolds numbers are defined as

$$\mathrm{Re} = \frac{u_{\rm rms}}{\nu k_R}, \ \mathrm{Re_M} = \frac{u_{\rm rms}}{\eta k_R}. \tag{12}$$

The SGS Prandtl and magnetic Prandtl number are given by

$$\mathrm{Pr_{SGS}} = \frac{\nu}{\chi_{\rm SGS}}, \ \mathrm{Pr_M} = \frac{\nu}{\eta}. \tag{13}$$

We note that the values of $\mathrm{Re_M}$ and $\mathrm{Pr_M}$ are given for the interior of the star. For the cases with different η in the exterior we consider two values, one in the inside and the other in the outside of the star. As in all numerical simulations of stellar convection the Prandtl is much larger and Reynolds numbers much smaller than in reality. The only effect that can be accurately modeled is the rotational influence measured by the Coriolis number; see, e.g. Käpylä et al. (2023).

3. Preliminary results

Figure 1 shows the evolution of the azimuthally averaged magnetic field $\overline{B}_\phi$ at the surface of the star as a function of time for the simulations of sets B and C. We choose simulations with each of our three setups: no diffusivity profiles, profile in the core, and profile in the core and exterior. The upper panel of the Fig. 1 shows the results for runs B1, B2, and B3. Run B1 with no diffusivity profiles has more cyclic fields near the equator toward the end of the simulation. In B2, for with a diffusivity jump inside the star, we see a quasi-static unipolar field superimposed with a cyclic pattern near the equator. In run B3, with diffusivity jumps inside and outside the star, the cycles disappear. In run C1, the dynamo is irregular and concentrated near the equator with sporadic activity with long quiescent periods. In run C3 we see regular cycles near the equator with a period about $P_{\rm cyc} = 21.7$ [yr]. Finally, run C4 has a quasi-static dynamo concentrated in the northern hemisphere.

Comparing the sets of runs, we notice similarities depending on the boundary conditions used. Runs B2 and C3 (with one jump) show similarity with the solar butterfly diagram, with C3 having the most regular cycles. On the other hand, runs B3 and C4 (with two jumps) have quasi-static dynamos, without polarity changes. A plausible reason for the differences in the dynamos depending on the diffusivity profiles is that if magnetic fields cannot penetrate (or they need more time to do so) the core and the exterior, the possible dynamo modes that can be excited will also be different from the case where uniform diffusion is used. This is most clearly seen in the case where a larger diffusivity is applied in the exterior of the star (runs B3 and C4) in which cases the cyclic solutions disappear. This can be understood as a lower excitation threshold for quasi-static solution in this geometry. It less clear why the dynamo in Run C1 operates only intermittently. A possibility is that the dynamo is only weakly supercritical for this combination of Ω and constant diffusivity. A more through

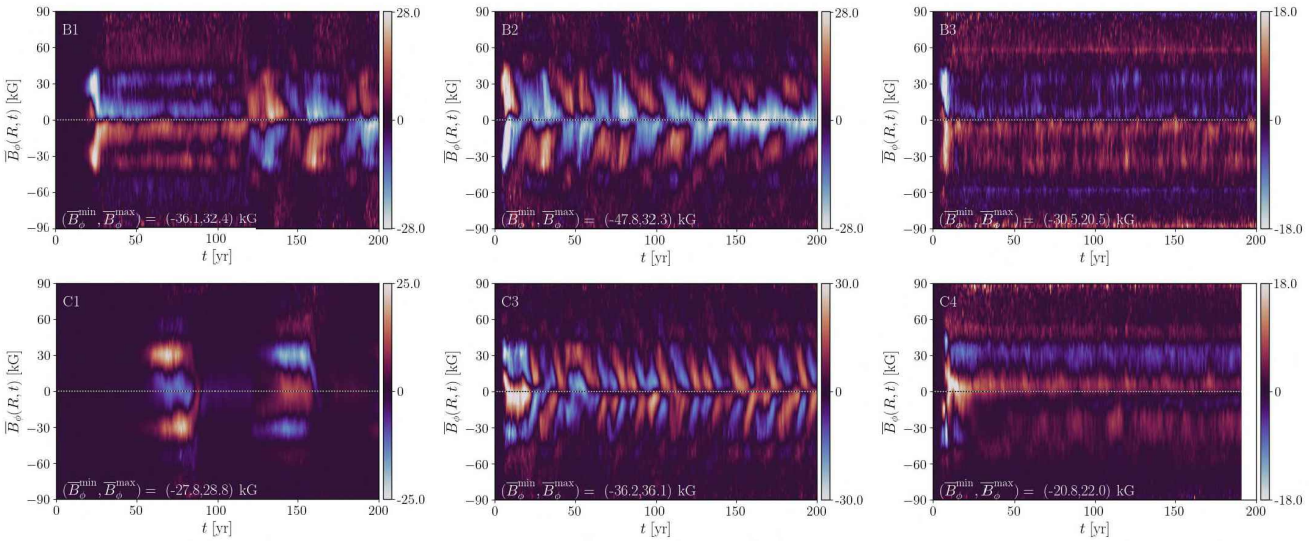

Fig. 1. Time-latitude diagrams of the mean toroidal magnetic field $\overline{B}_\phi(R,t)$ for a period of 200 yr for sets B and C. The y axes correspond to the latitude and the colour bar corresponds to $\overline{B}_\phi$ in kG. The dotted horizontal line indicates the equator. In the lower left corner is indicates the value of the magnetic field. *Upper panels:* Results for runs B1, B2 and B3 from left to right. *Lower panels:* Results for runs C1, C3 and C4 from left to right.

analysis in terms of mean-field dynamo theory is needed to ascertain the precises causes for the changing behavior.

We observe clear cycles only in runs C3 and toward the end of run B1. Longer time series is needed to ascertain this and whether the cycles in run B2 continue to fade away or whether they are robust. These issues will be revisited in a future study.

4. Summary and future work

It is clear that changing the conditions in the interior or exterior of the star, the large-sclae magnetic field is affected. In particular, enhancing the diffusivity exterior to the star leads to the disappearance of cyclic solutions. This is most likely due to different excitation conditions of cyclic and stationary dynamos depending on the spatial distribution of the diffusion coefficients.

In future work these results can be compared with the simulations of Ortiz-Rodríguez et al. (2023), who studied fully convective M dwarfs with the same model. This can be useful to explore what happens in the transition from fully convective to partially convective M dwarfs. As we already know the parameter regime where we obtain a dynamo, we will complete the set D and E with a simulation where the exterior magnetic boundary condition changes, and add another set (A) similar to sets D and E but with an $\Omega = 0.5$ to study how the magnetic field behaves over a considerable range of rotation rates. These simulations will be used to study the relation between stellar rotation and cycles.

Acknowledgements: We acknowledge the Kultrun Astronomy Hybrid Cluster via the projects Conicyt Quimal #170001, Conicyt PIA ACT172033, and Fondecyt Iniciacion 11170268. The support by the ANID BASAL project FB210003, and Fondecyt Regular (project code 1201280) and the Alexander von Humboldt - Foundation, Bonn, Germany. PJK was supported in part by the Deutsche Forschungsgemeinschaft (DFG, German Research Foundation) Heisenberg programme (grant No. KA 4825/4-1), and by the Munich Institute for Astro-, Particle and BioPhysics (MIAPbP) which is funded by the DFG under Germany's Excellence Strategy – EXC-2094 – 390783311.

References

Brandenburg A., 2007, Scholarpedia, 2, 2309
Brandenburg A., Nordlund A., Stein R.F., 2000, *Geophysical and Astrophysical Convection*, 85–105
Brown B.P., et al., 2020, ApJL, 902, L3
Chabrier G., Baraffe I., 1997, A&A, 327, 1039
Dobler W., Stix M., Brandenburg A., 2006, ApJ, 638, 336
Käpylä P.J., 2021, A&A, 651, A66
Käpylä P.J., 2022, ApJL, 931, L17
Käpylä P.J., et al., 2020, Geophysical and Astrophysical Fluid Dynamics, 114, 8
Käpylä P.J., et al., 2023, SSRv, 219, 58
Kochukhov O., 2021, A&A Rv, 29, 1
Navarrete F.H., et al., 2018, A&A, 615, A81
Navarrete F.H., et al., 2020, MNRAS, 491, 1043
Ortiz-Rodríguez C.A., et al., 2023, A&A, 678, A82
Paxton B., et al., 2019, ApJS, 243, 10
Pencil Code Collaboration, et al., 2021, The Journal of Open Source Software, 6, 2807
Warnecke J., et al., 2016, A&A, 596, A115
Winters J.G., et al., 2019, AJ, 157, 216